hiPSC-derived astrocytes from individuals with schizophrenia promote alterations in phagocytosis and chemotaxis of microglial-like cells

Pablo L. Cardozo[1], Chia-Yi Lee[2,#], Juliana P. S. Lacerda[1,#], Júlia S. Fahel[1], Pablo Trindade[3,10], Gabriela Vitória[3], Leonardo Chicaybam[4,5], Rafaela C. Cordeiro[1], Isaque J. S. de Faria[1], Nathália C. Silva[1], Yaovi M. H. Todjro[1], Joana C. do P. Maciel[3], Martin H. Bonamino[4,5], Luciene B. Vieira[6], Breno F. Cruz[7], Rodrigo Nicolato[7], Kristen J. Brennand[2,8], Stevens K. Rehen[3,9], Fabíola M Ribeiro[1,*]

1- Department of Biochemistry and Immunology, Institute of Biological Sciences (ICB), Universidade Federal de Minas Gerais (UFMG), Belo Horizonte, MG, Brazil; 2- Department of Genetics, Yale School of Medicine, Yale University, New Haven, CT, United States of America; 3- D'or Institute for Research and Education (IDOR), Rio de Janeiro, RJ, Brazil; 4- Molecular Carcinogenesis Program, Research Coordination, Instituto Nacional do Câncer (INCA), Rio de Janeiro, RJ, Brazil; 5- Vice-Presidency of Research and Biological Collections (VPPCB), Fundação Oswaldo Cruz (FIOCRUZ), Rio de Janeiro, RJ, Brazil; 6- Department of Pharmacology, Institute of Biological Sciences (ICB), Universidade Federal de Minas Gerais (UFMG), Belo Horizonte, MG, Brazil; 7- Department of Psychiatry, Faculty of Medicine, Universidade Federal de Minas Gerais (UFMG), Belo Horizonte, MG, Brazil; 8- Department of Psychiatry, Yale School of Medicine, Yale University, New Haven, CT, United States of America; 9- Department of Genetics, Institute of Biology, Universidade Federal do Rio de Janeiro (UFRJ), Rio de Janeiro, RJ, Brazil; 10- Current affiliation: Department of Clinical Analysis and Toxicology, Faculty of Pharmacy, Universidade Federal do Rio de Janeiro (UFRJ), Rio de Janeiro, RJ, Brazil

* Corresponding author: fmribeiro@icb.ufmg.br

[#] These authors contributed equally to this work.

ABSTRACT

Neuroinflammation, particularly astrocyte reactivity, are increasingly linked to schizophrenia (SCZ). Yet, the crosstalk between astrocytes and microglia in SCZ, especially under pro-inflammatory conditions, remains unclear. Here, we apply human induced pluripotent stem cells (hiPSCs) to compare the reactivity of astrocytes from individuals with SCZ and neurotypical controls, towards resolving how patient-derived astrocytes affect microglial biology. TNF-α stimulation of SCZ astrocytes, relative to control astrocytes, trigger an increase in expression of pro-inflammatory cytokines and CX3CL1, a chemokine involved in chemotaxis and synapse pruning. Transcriptomic analyses reveal that TNF-α-stimulated SCZ astrocytes promote the downregulation of biological processes associated with phagocytosis and chemotaxis in induced microglial-like cells (iMGs). Interestingly, TNF-α-stimulated SCZ astrocytes lead to reduced synaptoneurosomes engulfment by iMGs. Alternatively, TNF-α-stimulated astrocytes (control and SCZ) induce microglial migration in a CX3CR1-dependent manner. Surprisingly, TNF-α-stimulated SCZ astrocytes do not promote a more pronounced microglial chemotaxis, despite secreting twice as much CX3CL1 compared to stimulated control astrocytes, possibly due to lower CX3CR1 plasma membrane content after exposure to A_{CM} from individuals with SCZ. Altogether, these findings suggest that astrocytes contribute to SCZ pathology by altering normal microglial function.

INTRODUCTION

Schizophrenia (SCZ) is a neurodevelopmental disorder with an estimated lifetime prevalence ranging between 0.3-0.7% worldwide[1]. Symptom onset usually starts between late adolescence and early adulthood[2] and can be divided into three broad categories: positive symptoms (such as hallucinations, psychosis and delusions), negative symptoms (e.g., depressive behaviour, impaired speech, distraught thoughts and social withdrawn), and cognitive deficits (including working memory impairment, learning disabilities and attention deficits)[3-5].

The causes of SCZ remain poorly understood, as both genetic and environmental risk factors interact to generate susceptible conditions towards the onset of this multifactorial disorder later in life[6-9]. Environmental risk factors, including childhood stress, obstetric complications and maternal infection during pregnancy[7,9], trigger distinct inflammatory signalling cascades, which affect the developing brain at prenatal and early postnatal stages[6,8]. Indeed, genetic, transcriptional and serological evidence indicate increased inflammatory conditions in patients with SCZ, given the enhanced levels of multiple cytokines, such as enhanced levels of IL-1β, IL-6, IL-8 and TNF-α[8,10,11]. Moreover, genetic variants associated with SCZ show dynamic regulatory activity in neural cells in response to cytokine exposure[12].

Astrocytes provide metabolic support to neurons, facilitating the formation and modulation of synaptic connectivity, ionic buffering, and by uptaking and releasing neurotransmitters[13]. Along with microglia, astrocytes respond to pro-inflammatory stimulation through a wide range of receptors (e.g., Toll-like (TLR) and cytokine receptors), which, in turn, leads to their activation[14]. Astrocyte activation follows enhanced expression of reactivity markers, such as GFAP and Vimentin, as well as augmented secretion of cytokines and chemokines (e.g., TNF-α, IL-6, GM-CSF, TGF-β, CCL2)[13-15]. Secretion of these immune factors can, in turn, act upon microglial cells, either boosting or suppressing their activation, greatly impacting their effector capabilities, such as phagocytosis and cell migration[13-15]. Astrocytes also modulate microglial function under physiological conditions; for instance, astrocyte-produced IL-33 stimulates synaptic pruning by microglia, which is critical for proper neuronal connectivity[16].

Human genetic, post-mortem, and brain imaging analyses, together with mouse behavioural studies, link astrocytic dysfunction to SCZ[17,18]. Astrocyte and interferon-response gene expression modules were upregulated in patients with SCZ, while the microglia module was downregulated[19]. Likewise, PET-scans reveal increased astrocyte reactivity in individuals with SCZ in the anterior cingulate cortex and left hippocampus[20]. Finally, human induced pluripotent stem cells (hiPSCs)-derived astrocytes from individuals with SCZ have shown impaired astrocytic differentiation and maturation[21], abnormal calcium signalling[22], decreased glutamate uptake[22], reduced metalloproteinase activity[22] and enhanced pro-inflammatory profile[23,24].

Nonetheless, the crosstalk between astrocytes and microglia in SCZ, especially under pro-inflammatory conditions, remains unclear. Towards this, here we evaluate how reactive SCZ hiPSC-derived astrocytes affect microglial synaptic engulfment, chemotaxis and its transcriptional profile. We further assessed the contribution of CX3CL1/CX3CR1 axis involvement in these phenomena and aimed at identifying putative transcriptional factors driving the observed alterations.

RESULTS

SCZ-sourced astrocytes display increased pro-inflammatory profile following stimulation with TNF-α

Given the potential role for astrocytes in SCZ, we screened two transcriptomic (Szabo *et al*[22]; Akkouh *et al*[25]) and one proteomic (Trindade *et al*[23]) studies that compared gene/protein expression changes between hiPSC-derived astrocytes from individuals with SCZ and neurotypic controls (HCT), identifying common biological processes associated with all three datasets. Interestingly, only the GO:0019725 (cellular homeostasis) term overlapped among all three (**Supplementary Figure 1a-b; Supplementary Tables 1a-c**). Although no single gene candidate from the GO:0019725 term overlapped amongst all three studies, three genes were present in at least two: CX3CL1 (the sole member of the CX_3C chemokine family, also known as Fractalkine), NGFR (Nerve Growth Factor Receptor) and SLC24A2 (a calcium, potassium:sodium antiporter)

(**Supplementary Figure 1c-d**). CX3CL1 is associated with a wide range of biological processes that might be important in the context of SCZ, including microglial migration and synaptic pruning (**Supplementary Figure 1e**), the latter having long been hypothesised as a potential cause for this disorder[26]. Along with CX3CL1[27], classical complement components have also been implicated in synaptic elimination[28,29] (**Figure 1a**), while astrocyte-produced IL-33 has been shown to promote microglial-mediated synaptic uptake[16]. In addition, reactive astrocytes display increased expression of a wide range of cytokines with pleiotropic activities[13-15,30,31].

Taking in consideration the predicted involvement of inflammatory signalling in schizophrenia[8], we decided to assay the expression of CX3CL1, IL-33, complement components and pro- and anti-inflammatory cytokines in hiPSC-derived astrocytes from five neurotypic (HCT) and five SCZ cases, with and without pro-inflammatory stimulation with TNF-α (**Figure 1b**). Independent of donor diagnosis, CX3CL1 and C3 mRNAs were upregulated in astrocytes upon TNF-α stimulation, while C1q (subunit C) expression was not detected, and no change was observed in IL-33 and C4 expression (**Figure 1c-f**). Interestingly, CX3CL1 transcripts were more increased in stimulated SCZ astrocytes compared to stimulated controls (**Figure 1e**). Moreover, TNF-α stimulation promoted the mRNA upregulation of the pro-inflammatory cytokines TNF-α, IL-1α, IL-1β, IL-6, IL-8, and CCL5, while the mRNA of the anti-inflammatory cytokines IL-4 and IL-10 were not detected (**Figure 1g-l**). Noteworthy, stimulated SCZ astrocytes displayed significantly augmented IL-1α, IL-1β, IL-6 and CCL5 mRNA (and a trend towards increased TNF-α transcripts) levels compared to stimulated HCT astrocytes (**Figure 1g-k**). Taken together, these data indicate that SCZ astrocytes responded stronger to TNF-α stimulation by producing higher transcriptional levels of several pro-inflammatory cytokines and the chemokine CX3CL1, relative to HCT astrocytes.

TNF-α-stimulated SCZ astrocytes lead to the downregulation of chemotaxis and phagocytosis in microglial-like cells

Since many pro-inflammatory cytokines and CX3CL1 are pleiotropic, being capable of inducing several distinct functional responses in immune cells[31,32] (**Supplementary Figure 1e**), we queried potential biological processes that

might be altered in microglial-like cells by reactive SCZ astrocytes. We generated induced microglial-like cells (iMGs) from peripheral blood mononuclear cells (PBMCs) of a neurotypic individual (**Supplementary Figure 2**), incubated these cells with astrocyte conditioned media (A_{CM}) harvested from HCT and SCZ astrocytes subjected to either vehicle or TNF-α stimulation (**Figure 1b**), and applied bulk RNA-seq to evaluate the transcriptional profile of these iMGs.

Principal component (PC) analysis showed that iMG samples exposed to A_{CM} SCZ (+TNF-α) clustered separately from iMGs cultured with any other A_{CM} in PC1 (34.39%); otherwise, PC2 (18.04%) segregated iMGs incubated with A_{CM} HCT (+TNF-α) from all other samples. Only the third principal component (14.58%) effectively split samples based on A_{CM} sourced from either HCT or SCZ astrocytes **(Figure 2a)**. Larger transcriptional differences were observed when iMGs were exposed to A_{CM} from TNF-α-stimulated astrocytes. Indeed, 414 differentially expressed genes (DEGs) (326 up- and 88 downregulated) were identified in iMGs + A_{CM} HCT (+TNF-α), while 847 DEGs (388 up- and 459 downregulated) were found in iMGs + A_{CM} SCZ (+TNF-α), and only 110 DEGs (83 up- and 27 downregulated) were detected in iMGs + A_{CM} SCZ (N.S.) **(Figure 2b-c; Supplementary Tables 2a-c)**. Surprisingly, the iMGs + A_{CM} SCZ (N.S.) group had more DEGs in common with iMGs + A_{CM} HCT (+TNF-α) (51/110 DEGs) than with iMGs + A_{CM} SCZ (+TNF-α) (14/110 DEGs) **(Figure 2b)**. These data corroborate the PC analysis results, since the first two groups are clustered closer in PC1 compared to the latter **(Figure 2a).**

Gene-set enrichment analysis (GSEA) further explored the biological processes (GO terms) associated with each experimental condition. Incubation with either A_{CM} HCT (+TNF-α) or A_{CM} SCZ (N.S.) enriched similar GO terms. Indeed, both conditions promoted activation of immune response, response to pro-inflammatory cytokine stimulation, chemotaxis and immune cell migration **(Figure 2d; Supplementary Table 3a).** A closer inspection of the DEGs related to these upregulated GO terms unravelled the contribution of cytokines and chemokines (e.g., *CCL1, CCL5, CCL8, CXCL10, IL1A, IL1B*), immune receptors and downstream signalling transduction proteins (e.g., *ZAP70, SMAD3, JAK3, TREM1, IL2RA, IL2RB*) **(Figure 2e; Supplementary Table 3a).** On the other hand, downregulated GO terms diverged between these two groups. iMGs + A_{CM}

HCT (+TNF-α) showed negative enrichment for GO terms mainly involved in the endocytic processes, while iMGs + A_{CM} SCZ (N.S.) presented downregulation of biological processes related to mitochondrial metabolism **(Figure 2d; Supplementary Table 3a)**.

In marked contrast, GO terms associated with activation of immune response, chemotaxis and cell migration were negatively regulated in iMGs + A_{CM} SCZ (+TNF-α)**.** Additionally, biological processes related to endocytosis, phagocytosis and immune cell proliferation were also downregulated in this group (**Figure 2d, Supplementary Table 3a)**. A thorough investigation of DEGs associated to these downregulated GO terms revealed that some cytokines and chemokines, as well as immune signalling components (e.g., *CCL2, CCL7, CCL8, SMAD3, ZAP70,* and *JAK3*), which were upregulated in the other two groups, became either downregulated or did not display significant changes in expression when iMGs were incubated with A_{CM} SCZ (+TNF-α). Furthermore, many endocytic/phagocytic receptors (e.g., *MERTK, TREM2, CD93, MARCO*) also displayed decreased expression **(Figure 2e; Supplementary Table 2a)**. The only GO terms positively enriched in iMGs + A_{CM} SCZ (+TNF-α) were associated with mitochondrial metabolism, the opposite of what was observed for iMGs + A_{CM} SCZ (N.S.) **(Figure 2d; Supplementary Table 3a)**.

To confirm these results, we carried out GSEA using KEGG pathways. There was substantial convergence amongst upregulated pathways between iMGs + A_{CM} HCT (+TNF-α) and iMGs + A_{CM} SCZ (N.S.), particularly those concerning response to cytokines and chemokines **(Supplementary Figure 3; Supplementary Table 3b)**. On the other hand, some downregulated pathways, such as “Lysosome” and “Efferocytosis”, were found only when iMGs were exposed to A_{CM} from TNF-α-stimulated astrocytes (regardless of donor diagnostic background). Interestingly, the “phagosome” pathway was downregulated only in iMGs + A_{CM} SCZ (+TNF-α) samples, while pathways associated with neurodegenerative diseases were positively enriched in this group **(Supplementary Figure 3; Supplementary Table 3b).** Altogether, TNF-α-stimulated HCT and non-stimulated SCZ astrocytes induce similar transcriptional and biological processes alterations in iMGs, mainly regarding positive activation of immune response and chemotaxis. On the contrary, culturing microglia-like

cells in A_{CM} from TNF-α-stimulated SCZ astrocytes reversed this pattern, while also downregulating GO terms involved in phagocytosis.

Computation analyses unveil putative master regulators that potentially regulate cell migration and phagocytosis in iMGs

To gain better insight on how reactive SCZ astrocytes induce the downregulation of genes associated with chemotaxis and phagocytosis in iMGs, we undertook a systems biology approach to establish whether these genes are organised into recognizable co-expression modules. WGCNA resolved 35 modules **(Figure 3a; Supplementary Figure 4a-b).** GO term enrichment analysis identified the biological processes associated with each module, with the brown and blueviolet modules largely enriched for regulation of immune cells activation, cell migration, chemotaxis, phagocytosis and endocytosis **(Figure 3b-c; Supplementary Table 5).** Notably, these two modules were negatively correlated with iMGs incubated with A_{CM} SCZ (+TNF-α) and positively correlated with iMGs + A_{CM} SCZ (N.S.) **(Figure 3a).** Furthermore, the antiquewhite2 and lightgreen modules, positively correlated with iMGs + A_{CM} SCZ (+TNF-α) samples, were enriched for GO terms linked to mitochondrial metabolism **(Supplementary Figure 4c-d; Supplementary Table 5).** On the other hand, the darkolivegreen2 and palevioletred modules were positively correlated with iMGs cultured in the presence of A_{CM} HCT (+TNF-α) **(Figure 3a).** These two modules were mainly enriched for biological processes associated with response to cytokine and chemokine stimulation, as well as regulation of cytokine and chemokine production **(Figure 3d; Supplementary Figure 4e; Supplementary Table 5).** Altogether, these findings corroborate the GSEA results **(Figure 2d)** and indicate that genes involved in chemotaxis, cell migration and phagocytosis are mainly located in two co-expression modules (brown and blueviolet).

Co-expressed genes frequently share common regulators, such as upstream transcription factors (TFs). Therefore, we performed *in silico* master regulator analysis (MRA) using the human transcription factors (TFs)[33] as prospective regulators in our dataset. A total of 161 regulons were identified, of which 126 were shared between at least two groups, 5 were exclusive to iMGs + A_{CM} HCT (+TNF-α) and 30 solely pertained to iMGs + A_{CM} SCZ (+TNF-α) **(Supplementary Figure 5a; Supplementary Tables 6a-c).** Next, we calculated

the predicted activity status of these transcription factors and only kept those whose activity were either activated or repressed in at least one experimental group **(Supplementary Figures 5b-d and 6; Supplementary Tables 6a-c)**. To assess the putative TFs regulating the co-expressed gene networks, we carefully cross-examined the target genes of each regulator and the gene sets of the WGCNA modules. IRF1, whose activity status was predicted to be activated and was the only TF exclusive to iMGs + A_{CM} HCT (+TNF-α) **(Supplementary Figure 5b)**, was associated with the darkolivegreen2 module **(Figure 3e)**, pointing to its possible role in inducing the expression of genes involved in the response to cytokine and chemokine stimulation in this group. Interestingly, we found four (HHEX, SOX4, MEF2C and NFATC2) and two (CENPA and MXD3) TFs connected to the brown and blueviolet modules, respectively **(Figure 3e).** Moreover, except for SOX4, these putative TFs had a predicted repressed activity in the iMGs + A_{CM} SCZ (+TNF-α) group **(Supplementary Figures 5d and 6)**, which could indicate their participation in triggering the downregulation of genes associated with chemotaxis, cell migration and phagocytosis.

Reactive SCZ astrocytes lead to reduced synaptic material engulfment by iMGs

Given that activated HCT and SCZ astrocytes significantly perturbed transcription of chemotaxis, cell migration, and endocytosis/phagocytosis genes in microglial-like cells, we revisited our initial screening results to select a target that could modulate these processes **(Figure 1)**. We prioritized the role of CX3CL1 in SCZ, as it is involved in synapse elimination, microglial cell migration and chemotaxis, and also showed increased mRNA expression in TNF-α-stimulated SCZ astrocytes relative to stimulated controls **(Supplementary Figure 1e; Figure 1e)**. In that way, we initially sought to validate CX3CL1 mRNA expression findings at the protein level. TNF-α stimulation increased the production and secretion of CX3CL1 in both HCT and SCZ astrocytes, while no change in expression was observed in non-secreted CX3CL1 **(Figure 4a-c)**. Remarkably, stimulated SCZ astrocytes showed an approximate two-fold augmentation in secreted CX3CL1 levels compared to stimulated control astrocytes **(Figure 4c).**

To ask whether SCZ astrocytes impact synaptic material engulfment by iMGs and to evaluate CX3CL1 role in this phenomenon, synaptoneurosomes were isolated from mature hiPSC-derived neurons **(Supplementary Figure 4a-e)**, fluorescently labelled, and added to control iMGs, in the presence or absence of recombinant CX3CL1 (rCX3CL1) for 24 h **(Supplementary Figure 4f-i).** It was observed that rCX3CL1 diminished synaptoneurosomes uptake by iMGs **(Supplementary Figure 4h-i).**

Considering this result, we tested whether astrocyte conditioned media (A_{CM}) from reactive SCZ astrocytes required CX3CL1 signalling to lessen iMG phagocytosis. Pharmacological blockade of CX3CR1 with AZD8797, prior to incubation with A_{CM} and synaptoneurosomes **(Figure 4d-f)**, increased synaptoneurosomes uptake in control conditions (A_{CM} HCT (N.S.)) relative to vehicle-treated iMGs**.** Incubation with A_{CM} SCZ (+TNF-α) was the only condition capable of attenuating synaptic engulfment by iMGs**.** However, inhibition of CX3CR1 did not prevent this reduction in synaptoneurosome phagocytosis, suggesting that CX3CL1 was not responsible for triggering the observed phenotype. Additionally, while incubation with A_{CM} HCT (+TNF-α) or A_{CM} SCZ (N.S.) did not promote significant alterations in synaptoneurosome engulfment relative to vehicle-treated iMGs exposed to A_{CM} HCT (N.S.), pharmacological blockade of CX3CR1 did not enhance synaptic material uptake by iMGs in such conditions **(Figure 4e-f).** Overall, these data suggest that reactive SCZ astrocytes hinder microglial synaptic material phagocytosis. Furthermore, under reactive conditions, A_{CM} effects on iMGs were CX3CL1-independent, not being reversed by the pharmacological inhibition of its receptor.

TNF-α-stimulated astrocytes induce microglial migration

Given the CX3CL1 involvement in cell migration and its increased secretion by reactive SCZ astrocytes (**Figure 4c; Supplementary Figure 1e**), we next queried whether SCZ astrocytes altered microglial migration**.** Here, microglial exposure to A_{CM} from TNF-α-stimulated HCT and SCZ astrocytes significantly enhanced microglial migration, in a CX3CR1-dependent manner **(Figures 5a-b)**. Unexpectedly, although reactive SCZ astrocytes secreted almost twice as much CX3CL1 relative to their HCT counterparts, there were no differences in their capacity to induce microglial chemotaxis **(Figures 5a-b).**

Finally, we measured the total and plasma membrane content of CX3CR1 in iMGs exposed to A_{CM} for 24 h. SCZ astrocyte conditioned media (but not HCT, regardless of stimulation status) diminished CX3CR1 plasma membrane content in iMGs, while total CX3CR1 levels remained unchanged **(Figure 5c-d)**. Taken together, these results indicate that both transcriptional repression of chemotaxis-related biological processes and diminution of CX3CR1 plasma membrane levels prompted by reactive SCZ astrocytes act in concert to restrict microglial-like cells migratory capabilities.

DISCUSSION

Multiple lines of evidence link microglia and astrocytes to the neuropathological mechanisms implicated in SCZ[19-23,34,35], yet little is known about how these glial cells communicate and regulate each other's function in this disorder. Here, we applied a combination of functional assays and transcriptomics to determine how SCZ astrocytes modulate key aspects of microglial biology. SCZ astrocytes displayed a stronger response to pro-inflammatory stimulation and downregulated processes linked to immune cell activation, phagocytosis, cell migration and chemotaxis in iMGs. In addition, CX3CL1 was secreted at higher levels by stimulated SCZ astrocytes. Meanwhile, decreased microglial synaptoneurosome engulfment following incubation with A_{CM} SCZ (+TNF-α) was CX3CR1-independent, whereas increased microglial migration was CX3CR1-dependent.

Although decreased synaptoneurosome phagocytosis following incubation with A_{CM} SCZ (+TNF-α) could challenge the long proposed hypothesis of increased synaptic pruning in SCZ[26], other evidence must also be considered. Indeed, Sellgren *et al*[36] showed that SCZ iMGs display enhanced synaptic engulfment in a cell-autonomous fashion. Additionally, the same study demonstrated that hiPSC-derived neurons, from individuals with SCZ carrying the *C4A* risk allele[37], exhibit augmented C3 deposition and, consequently, more synaptic uptake by iMGs. Moreover, Yilmaz and colleagues[29] revealed that overexpression of human *C4A* in mice leads to microglia-mediated excessive synapse loss in the medial PFC. It should be recalled that complement tagging is

a downstream consequence of reduced synaptic activity[28] and that GWAS reports already pointed that several risk *loci* indicate that dysfunctional synaptic transmission may occur in this disorder[38]. Therefore, we propose that the hypothetical excessive synaptic pruning in SCZ relies mainly on preexisting synaptic dysfunction and on microglial cell autonomous mechanisms. Nevertheless, we should not completely disregard astrocyte participation, given that the results presented here might indicate that astrocytes could have a compensating role by reducing excessive pruning by microglia.

Given that CX3CR1 mRNA is downregulated in the blood and brain of patients with SCZ[19,39,40], with a $CX3CR1^{A55T}$ loss of function variant identified as a SCZ risk factor[39], we suggest that activated astrocytes contribute to the CX3CL1/CX3CR1 axis dysfunction in SCZ. Yet, another seeming contradiction in our results is that TNF-α-stimulated SCZ astrocytes secreted twice the amount of CX3CL1 compared to HCT counterparts, but they did not induce a stronger migratory response in iMGs. One possible explanation is the reduced cell surface content of CX3CR1 in iMGs incubated with ACM SCZ (+TNF-α). There may be alternate pathways that result in transcriptional downregulation of chemotaxis and cell migration as well, as indicated by our results. Notwithstanding, these results should be viewed as part of a grander change in the immune response landscape of these microglial-like cells. Indeed, while iMGs incubation with A_{CM} HCT (+TNF-α) or A_{CM} SCZ (N.S.) exhibited the upregulation of several biological processes that favour immune activation (e.g., response to cytokines and chemokines; immune cell activation and proliferation; chemotaxis and cell migration), the opposite is solely observed when these same cells are exposed to A_{CM} SCZ (+TNF-α). These results strengthen the hypothesis that SCZ development requires the simultaneous presence of a susceptible genetic background and external stimuli[8].

Intriguingly, the downregulation of processes associated with immune responses, along with the increased mRNA expression of certain genes (e.g., *IL1B, MMP12* and *SERPINE1*) and the reduced phagocytic and migratory capacity shown by microglia exposed to A_{CM} SCZ (+TNF-α) share remarkable features with cellular senescence hallmarks[41-43]. Supporting this hypothesis, *post-mortem* findings reported augmented lipofuscin granules in microglia from

younger and older individuals with SCZ, another characteristic cellular senescence feature[35,44]. In addition, it has already been demonstrated that patients with SCZ display older biological brain age relative to controls or when compared to their own chronological age[45-47]. Hence, it could be speculated that reactive SCZ astrocytes trigger accelerated microglial aging, leading them to a senescent-like state[48].

We employed computational methods to identify putative master regulators capable of promoting the microglial phenotypic transition observed here. We identified five transcription factors (MEF2C, NFATC2, HHEX, CENPA and MXD3), whose activity are predicted to be repressed solely in the iMGs + A_{CM} SCZ (+TNF-α) condition. Our data show that these TFs are likely responsible for regulating the expression of genes associated with immune cell activation, chemotaxis, cell migration and phagocytosis. Intriguingly, MEF2C, NFATC2 and HHEX have already been implicated in SCZ[49-53]. On the other hand, this is the first report to date to provide evidence for the potential involvement of CENPA and MXD3 in this disorder. These data suggest a potential mechanism pointing to putative upstream regulators that can explain, at least in part, the observed reduction in synaptoneurosome phagocytosis and the restricted migration of microglial cells even in the presence of higher levels of chemotactic cues. However, a thorough characterization about how each TF affect microglia in the context of SCZ is out of the scope of this work.

Despite the relevance of the data shown here, some limitations of this work remain. Firstly, while we have provided strong evidence that reactive SCZ astrocytes affect several immune related processes in microglial-like cells (mainly cell migration and phagocytosis), the same set of experiments should be conducted using microglia obtained from patients with SCZ to have a more complete picture of the crosstalk between these two glial cell types in the context of this disorder. Secondly, it is not entirely clear what developmental time frame is modelled in this study (i.e., whether our findings recapitulate events that take place before or after symptom onset). Further research using more suitable developmental models, such as those employing microglia-containing organoids from individuals with SCZ, should be carried out to address this point.

In summary, our results demonstrate that activated SCZ astrocytes lead to substantial alterations in microglial biology, both at functional and transcriptional levels. Moreover, our data provide new avenues of investigation that should be subject of future studies, such as whether the master regulators identified in this work could also comprise valuable targets for future therapeutic strategies to prevent or treat SCZ.

MATERIALS AND METHODS

Materials and reagents

A complete list of all materials and reagents used in this study can be found in the **Supplementary Table 7.**

hiPSC-derived astrocytes differentiation

Astrocytes were differentiated from hiPSCs sourced from five controls and five individuals with SCZ (**Supplementary Table 8**), as previously described[30,54]. Once hiPSC-derived neural stem cells (NSCs) reached 90% confluency, cells were dissociated with Accutase and seeded at 5 x 10^4 cells/cm^2 in Geltrex-coated TC 25 cm^2 flasks in Astrocytes Differentiation Medium (DMEM/F-12, 1x N-2 supplement, 1% Heat-inactivated Foetal Bovine Serum (FBS) and 1% 1% antimycotic-antibiotics solution (anti-anti)). Media was replenished every other day for 21 days. Whenever differentiating astrocytes reached full confluency, cells were expanded to larger Geltrex-coated TC flasks at 1:3 ratio as described. By the end of this differentiation period (day 21), media was switched to Astrocytes Maturation Medium (DMEM/F-12, 10% FBS and 1% anti-anti) to mature astrocytes for 5 weeks. Whenever astrocytes reached full confluency, they were split using Trypsin/EDTA 0.125% solution (diluted in PBS $1x^{-/-}$) and expanded to 175 cm^2 TC flasks without Geltrex coating at 1:2 ratio to negatively select undifferentiated non-adhering cells. Cells were cultured in standard conditions. Astrocytes' identity was confirmed by positive immunostaining to EAAT1, Vimentin, GFAP and Connexin 43 **(Supplementary Figures 9A-B).**

Astrocytes Stimulation

After at least 5 weeks of maturation, astrocytes were detached using Trypsin/EDTA 0.125% solution, pelleted down by centrifugation (800 g for 5 min), resuspended in Astrocytes Maturation Medium and plated at 1.25 x 10^4 cell/cm^2 density in either TC 6-well plates or 25 cm^2 flasks. After 5 days in culture, cells were washed three times with PBS $1^{-/-}$ and serum-starved for 24 h in DMEM/F-12 supplemented with 1% anti-anti. Next, astrocytes were stimulated for 24 h with 10 ng/mL recombinant human TNF-α or vehicle (0.1% BSA solution). Once stimulation finished, astrocytes conditioned media (A_{CM}) was collected, clarified by centrifugation (3000 g, 4 °C for 10 min), flash frozen and stored at -80 °C until further use. In addition, astrocytes monolayers were harvested either in TRIzol reagent according to manufacturer instructions or in RIPA lysis buffer containing protease and phosphatase inhibitors for 1 h on ice and stored at -80 °C.

Total RNA extraction and RT-qPCR

Total RNA was isolated using the TRIzol reagent as per manufacturer instructions and resuspended in 12 µL DEPC-treated nuclease-free water. RNA concentration and quality (260/230 and 260/280 ratios) were analysed by spectrophotometry in the Multiskan GO (Thermo Scientific). 1 µg total RNA was reverse transcribed in a reaction mixture consisting of 15 ng/µL Random Primers, 50 mM Tris-HCl, 75 mM KCl, 3 mM $MgCl_2$, 625 µM dNTPs, 10 µM DTT and M-MLV reverse transcriptase. Reverse transcription conditions were as follows: (Random primers annealing) 70 °C for 10 min and 4 °C for 10 min; (cDNA extension) 42 °C for 60 min and 70 °C for 15 min. The resulting cDNA was diluted 1:10 in nuclease-free water and subjected to qPCR using Power SYBR Green PCR Master Mix and 200 nM of forward and reverse primers mix (sequences available in **Supplementary Table 9**) in the QuantStudio 7 System (Applied Biosystems). Thermal cycling conditions were: 50 °C for 2 min, 95 °C for 10 min; 40 cycles of 95°C for 15 s and 60 °C for 1 min; followed by melting curve analysis. All primers pairs had 90-110% efficiency. Relative gene expression of target genes was normalised by the average of housekeeping genes (RPLP0 and IPO8) and calculated by the $2^{-\Delta Ct}$ method.

Enzyme-linked Immunosorbent Assay (ELISA)

Soluble CX3CL1 was quantified in A_{CM} using the Human CX3CL1/Fractalkine DuoSet ELISA kit as per manufacturer instructions. Astrocytes monolayers of all cell lines were detached using Trypsin/EDTA 0.125% solution and counted in a haemocytometer shortly after A_{CM} harvest to normalise data by cell count.

Synaptoneurosomes isolation

Synaptoneurosomes isolation was performed as described by Sellgren *et al* (2017)[55] with minor modifications. After 60 days of differentiation, media was removed from neuronal cultures and replaced by non-stimulated A_{CM} from their isogenic counterparts 24 h before cell harvest. Next, media was thoroughly removed, and cells washed twice with ice-cold PBS 1x. 1 mL per 100-mm petri dish of ice-cold Synaptoneurosomes Isolation Buffer (SIB; 10 mM HEPES, 1 mM EDTA, 2 mM EGTA, 0.5 mM DTT and protease inhibitors; pH 7.0)[56] was added and neurons gently scrapped. This cell suspension was transferred to a sterile 1.5 mL conical tube and centrifuged at 1,200 g for 10 min at 4°C. The supernatant (homogenate) was transferred to a new sterile 1.5 mL conical tube and centrifuged at 15,000 g for 20 min at 4 °C. Finally, the supernatant (cytosolic fraction) was removed, pelleted synaptoneurosomes resuspended in SIB with 5% DMSO and frozen at -80 °C until further use. Aliquots of each fraction were collected at each step for further characterization by Western Blot and stored at -80 °C. Freshly isolated synaptoneurosomes were also plated overnight on 13-mm acid-etched glass coverslips coated with 50 µg/mL poly-D-lysine solution and left to attach overnight under standard culture conditions for further immunostaining to Syntaxin 1 and Homer. Shortly before the phagocytosis assay, synaptoneurosomes were homogenised for up to 50 times in ice-cold PBS 1x using a sterile micro-capillary pipet tip, its concentration adjusted to 0.25 µg/µL and labelled with 2 µM Vybrant-CM-DiI, as per manufacturer instructions.

Donor selection and PBMCs isolation

A male control individual was chosen (**Supplementary Table 8**), after evaluation by a trained psychiatrist following the M.I.N.I. 7.0.0[57] and fitting the following inclusion and exclusion criteria: less than 50 years of age; at least high school education; no previous history of neurological or neuropsychiatric

conditions; without 1st degree relatives diagnosed with psychiatric disorders; without 2nd degree relatives diagnosed with SCZ, bipolar disorder or autism spectrum disorder; non-cannabis user; non-smoker; capability to freely and voluntarily give informed consent to participate in this study. Whole blood was drawn from this individual, diluted 1:1 with PBS $1x^{-/-}$, carefully layered onto Histopaque 1077 density gradient and centrifuged at 900 g for 25 min (with acceleration and braking settings turned off). After blood fractionation, the PBMCs layer was collected using a sterile plastic Pasteur pipette, resuspended in PBS $1x^{-/-}$ and centrifuged at 400 g for 8 min. The supernatant was removed, cells resuspended once again in PBS $1x^{-/-}$ and pelleted by centrifugation at 400 g for 8 min. PBMCs were resuspended in FBS, counted in a haemocytometer and cryopreserved in FBS + 10% DMSO for later use.

Induced microglial-like cells (iMGs) differentiation

PBMCs were differentiated in iMGs as described elsewhere[55,58]. PBMCs were plated in either 13-mm acid-etched glass coverslips or TC-treated plasticware, both previously coated overnight with Geltrex, in RPMI 1640, supplemented with 10% FBS and 1% penicillin-streptomycin (P/S) solution. Cell density was adjusted on an assay-dependent basis. In the following day (day 0), media was completely switched to iMG differentiation media (MDM), comprised of RPMI 1640, 1% Glutamax, 100 ng/mL IL-34, 10 ng/mL GM-CSF and 1% P/S. On the 6th day of differentiation, half of media was changed and replenished by fresh MDM. On day 9, media was thoroughly removed, cells washed twice with pre-warmed RPMI 1640 to remove cell debris and fresh MDM added. iMGs were used for subsequent experiments between days 10-12 of differentiation. iMGs were kept in standard culture conditions. Microglial-like identity was confirmed by cells bearing ramified morphology and positive immunostaining to CX3CR1, Iba1 and Pu.1. Bright-field images were captured using the FLoid Cell Imaging Station (Thermo Fisher).

Synaptoneurosomes phagocytosis assay

2.8×10^5 PBMCs/cm^2 per well were seeded in 24-well plates and differentiated as already described. On day 12, iMGs were incubated for 1 h with 2 ng/mL recombinant CX3CL1 or vehicle (0.1% BSA solution). Alternatively, iMGs

were pre-treated with 5 μM AZD8797 or vehicle (DMSO) for 1 h; then, half of the media was removed and replenished by an equal volume of pooled A_{CM} and cells incubated for another hour (AZD8797 was also added again to ensure its concentration was kept at 5 μM throughout the whole experiment). Next, 1.875 μg of CM-DiI-labelled synaptoneurosomes were added to each well, plates gently shaken for thorough homogenization and incubated for 24 h in standard culture conditions in the Cytation 5 Cell Imaging Multi-mode Reader (BioTek; CAPI - ICB, UFMG, Brazil). Four equally spaced image sets (bright field and RFP channels) per well were captured every two hours. Experiments were conducted twice in duplicates to ensure reproducibility. After 24 h, images were retrieved and analysed using the combination of the following open-source softwares: (1) *FIJI/ImageJ* (v. 1.54f) for brightness/contrast adjustments and denoising; (2) *fastER*[59] (v. 1.3.5) for cell segmentation (bright field channel); (3) *CellProfiler*[60] (v. 4.2.1) for single-cell phagocytic index quantification (pipeline available in **Supplementary File 1**). Phagocytic index was calculated as the ratio of red object area (μm^2) inside a given cell by its total cell area (μm^2). Orthogonal projection (z-step: 2 μm; number of steps: 20) was generated using *FIJI/ImageJ* from vehicle-treated (0.1% BSA) fixed samples (24 h time-point) on glass coverslips immunostained for Alexa 633 Phalloidin and Hoechst 33342 as described.

Cell-based ELISA

5.26×10^5 PBMCs/cm^2 per well were plated in Geltrex-coated TC 96-well plates and differentiated to iMGs as described. Once differentiation was completed, half of media was removed, replenished by an equal volume of pooled A_{CM} and incubated for 24 h in standard culture conditions. Afterwards, media was carefully removed, and cells fixed with 4% PFA solution (in PBS 1x) for 15 min. Then, cell-based ELISA was carried out based on Yang *et al* (2021)[61] with modifications. Samples were washed three times with PBS 1x for 5 min under gentle agitation to remove excessive fixative solution. Next, for total CX3CR1 measurements only, PBS 1x was removed and replaced by permeabilizing solution (0.1% Triton X-100 in PBS 1x) for 10 min; for plasma membrane CX3CR1 measurements, samples were incubated with PBS 1x (without Triton X-100) for an equal time. Once this incubation was over, intracellular peroxidases

were quenched by incubation with 1% H_2O_2 (in PBS 1x) for 20 min. Quenching solution was removed and samples blocked with 1% BSA (in PBS 1x) for 1 h at room temperature. Blocking solution was discarded and cells incubated with anti-CX3CR1 (1:500; diluted in blocking solution) overnight, at 4 °C and the plate sealed with parafilm to prevent evaporation. In the following day, primary antibody solution was removed, samples washed thrice as described and incubated with HRP-conjugated anti-rabbit IgG (1:2000) for 2 h, at room temperature and protected from light exposure. Secondary antibody solution was removed, washed as described and samples incubated with the substrate solution (0.4 mg/mL OPD, 0.8 µL/mL in citrate buffer (111.2 mM NaH_2PO_4, 27 mM citric acid, pH 5.0)) for 30 min, at room temperature and protected from light. Chromogenic reaction was stopped by adding 5.5% H_2SO_4 solution to each well and absorbance measured after 5 min at 490 nm in the Multiskan GO plate reader (Thermo Fisher). For whole cell staining, the chromogenic solution was removed, cells washed five times with PBS 1x as described and incubated with 1% crystal violet solution for 30 min under gentle agitation. Crystal violet solution was removed, samples washed extensively with ddH_2O to remove excessive amounts of dye, washed thrice with PBS 1x as described and incubated with 1% SDS solution for 1 h, under agitation, to solubilize intracellular crystal violet. Absorbance was read at 595 nm in the plate reader and this measurement used to normalise CX3CR1 protein levels, according to the formula below:

$$Relative\ Protein\ Levels\ (RPL) = \frac{OD_{490}\,Sample - OD_{490}\,Blank}{OD_{595}\,Sample - \ OD_{595}\,Blank}$$

RPL was expressed relative to iMGs exposed to A_{CM} HCT (N.S.). Experiments were conducted twice with five replicated each.

cDNA library preparation and sequencing

4.0 x 10^5 PBMCs/cm^2 per well were seeded in Geltrex-coated TC 12-well plates and differentiated as described. After 12 days of differentiation, half of media was discarded and replaced by an equal volume of pooled A_{CM}. 24 h later, media was completely removed, and cells harvested in TRIzol reagent. Total RNA extraction was performed as recommended by the manufacturer and RNA quality analysed in the 2100 Bioanalyzer platform (Agilent). 200 ng of total RNA (RIN > 7) was subjected to rRNA depletion and cDNA library preparation using

the NEBNext Ultra II Directional RNA Library Prep Kit, according to manufacturer instructions. cDNA library quality assessment and paired-end sequencing (2 x 100 pb) using the NextSeq2000 platform (Illumina) was performed by the LaCTAD (UNICAMP, Brazil). Samples had an average sequencing coverage of 30 million reads/library.

RNA-seq data processing and differential gene expression analysis

RNA-seq reads quality was assessed by *FastQC.* Adaptor sequences were trimmed out and reads with less than 50 bp or Phred < 20 were removed using *Trimmomatic* (v. 0.40). The *STAR* aligner (v. 2.7.11b) was used for mapping reads to the human reference genome (GRCh38), and *featureCounts* (v. 2.0.6) was employed to count mapped reads. Features with fewer than 10 counts were excluded from further analysis. Batch effects were removed using the *RUVseq* package (residuals method; v. 1.34.0). *edgeR* (v. 3.42.4) was employed for differential gene expression analysis (adjusted p-value < 0.05; $|\log_2 FC| \geq 0.5$). Principal component analysis was performed using the *PCAtools* package (v. 2.12.0).

Gene-set enrichment analysis (GSEA)

Lists of ranked genes, from the differential gene expression analysis results, were generated using the following criterium: sign ($\log_2$ FC) * ($-\log_{10}$ p-value). Next, these ranked lists were subjected to GSEA using the *clusterProfiler* package (v. 4.8.3) to identify enriched GO Biological Processes and KEGG Pathways.

Weighted Gene Co-expression Network Analysis (WGCNA)

For WGCNA, batch-effects were removed and normalised read counts obtained using *RUVseq*. Genes with fewer than 10 counts were excluded, and the top 10,000 genes with the highest variance were selected for network construction. A soft thresholding power of 11 was applied using the signed-hybrid network type. The minimum module size was set to 30, and modules were merged if their Spearman correlation coefficient exceeded 0.8. Correlation p-values were adjusted using the Benjamini and Hochberg method (adjusted p-value < 0.05). The *bioNERO* package (v. 1.8.7) was used alongside *WGCNA* (v.

1.72-5) for analysis and visualisation. GO term enrichment analysis was performed using the *biomaRt* package (v. 2.56.1).

Master Regulator Analysis (MRA)

MRA analysis was carried out based on the pipeline published by Leng *et al* (2022)[62] with adaptations, using the *RTN* package (v. 2.24.0). Firstly, for co-expression network reconstruction, 871 RNA-seq datasets were downloaded from ARCHS4[63], whose sample descriptors were “Microglia” and “Human”. Batch effects across datasets were removed using the *Combat-seq* function of the *sva* package (v. 3.48.0), gene counts log transformed using the *vst* function of the *DESeq2* package (v. 1.40.2) and gene-level count matrix subset to contain only the 16,954 genes identified in the RNA-seq dataset of the present study. The list of human transcription factors published by Lambert *et al* (2018)[33] was inputted as regulatory elements for network reconstruction. After transcriptional regulatory network reconstruction finished, master regulators and their activity status for each experimental condition were calculated as described in the *RTN* package vignette (adjusted p-value < 0.1). Associations between activated or repressed regulons and WGCNA modules were done using the *tni.overlap.genesets()* function.

iMGs migration assay

3.8 x 10^5 PBMCs/cm^2 were plated in Geltrex-coated 60-mm TC petri dishes and differentiated as already described. After 9 days of differentiation, iMGs were pre-treated with 10 µM Rho-kinase inhibitor Y-27632 for 1 h, followed by incubation with hypertonic citrate saline solution (135 mM KCl and 15 mM sodium citrate diluted in PBS 1x) for 5 min at 37 °C to gently loosen up attached cells. Next, iMGs were gently scraped using a cell scraper, collected into a 15 mL conical tube (pre-coated with sterile 5% BSA solution, overnight at 4°C) and centrifuged at 400 g for 8 min. Supernatant was discarded, iMGs resuspended in MDM and 6.0 x 10^4 cells/transwell plated into the upper compartment of each Geltrex-coated transwell. 24 h after plating, iMGs were pre-treated with AZD8797 (5 µM) or vehicle (DMSO) for 1 h, before pooled A_{CM} was added in the lower compartment and incubated overnight (~ 16 h) in standard culture conditions. In the next day, iMGs migration was stopped by fixing these cells for 15 min with

4% PFA. Transwells were washed three times with PBS 1x, non-migrated cells (in the upper compartment) gently scraped off using a cotton swab and migrated cells (in the lower compartment) stained with Hoechst 33342 (1:500; diluted in PBS 1x) for 10 min and protected from light. Samples were washed as described and subsequently imaged in the EVOS FL Color microscope (Thermo Fisher). 4-5 image fields/transwell were randomly acquired and migrated cells quantified by a trained researcher, blind to the experimental conditions, using the *CellCounter* plugin on *FIJI/ImageJ*. Migrated cell count was expressed as percentage relative to vehicle-treated iMGs exposed to A_{CM} HCT (N.S.). This experiment was executed three times independently.

Ethics Statement

All experiments carried out throughout this work has been approved by UFMG's Ethics Committee (COEP-UFMG; protocol number: 90424518.3.1001.5149) and were performed according to the Helsinki Declaration and the Brazilian National Health Council Resolution 466/12.

Data availability

Raw and normalised gene-level count data, and R markdown files can be found in https://github.com/plcardozo/Cardozo-et-al---iMG-transcriptomics. Unprocessed sequencing files and other data may become available upon request.

Supplementary Methods

A detailed description about candidate genes screening, NSCs[30,54] and neuronal[64] differentiation from hiPSCs, western blot and immunostaining protocols, *Mycoplasma* testing[65] and statistical analyses performed in this study can be found in the **Supplementary Information** file.

ACKNOWLEDGEMENTS

We acknowledge the contributions on technical support of Mr. Jamil Silvano de Oliveira, Mr. Samuel Tadeu Rocha, Mr. Leandro Costa Nascimento, Dr. João Trindade Marques, all current and former members of the Laboratory of

Neurobiochemistry (UFMG, Belo Horizonte, Brazil) and all medical and nursery personnel at the Borges da Costa Clinic (UFMG Clinic's Hospital, Belo Horizonte, Brazil). We also thank Dr. João Paulo Pereira de Almeida, Dr. Álvaro Gil Araújo Ferreiro and Ms. Sophie Turetsky Cohen for their valuable discussions and insights regarding this work. This research project was funded by Conselho Nacional de Desenvolvimento Científico e Tecnológico (CNPq) grants 441719/2020-1 and 403171/2023-7 and Fundação de Amparo à Pesquisa do Estado de Minas Gerais (FAPEMIG) grants APQ-03921-22 and APQ-00140-23. P.L.C. was recipient of CNPq and Fulbright scholarships during this work and is currently recipient of CAPES/Print fellowship; J.P.S.L. and N.C.S. are recipients of CNPq graduate scholarships.

AUTHORS CONTRIBUTIONS

P.L.C. and F.M.R. conceived and designed the study. P.L.C. performed candidate genes screening, total RNA extraction, hiPSCs-derived neurons characterization, synaptoneurosomal characterization, iMGs synaptoneurosomes engulfment analysis pipeline development and quantification, western blots, ELISA, cell-based ELISA and iMGs migration assay. G.V. differentiated hiPSCs to NSCs. G.V. and J.C.P.M. characterized hiPSCs and NSCs. P.L.C., J.P.S.L. and P.T. differentiated hiPSC-derived astrocytes. P.T. characterized hiPSC-derived astrocytes. P.L.C. and J.P.S.L. performed astrocytes stimulation, RT-qPCR experiments, hiPSC-derived neuronal differentiation, iMGs differentiation and characterization. P.L.C. and J.S.F. performed synaptoneurosomes isolation and synaptoneurosomal phagocytosis assay. J.P.S.L. carried out iMGs migration assay blind quantification. B.F.C. performed PBMC's donor psychiatric evaluation. R.N. supervised PBMC's donor candidate recruitment and helped to draft ethics committee protocol. N.C.S. drew whole blood from healthy control donor. P.L.C., N.C.S. and R.C.C. performed PBMCs isolation from whole blood. R.C.C. and J.S.F. helped in standardizing ELISA and cell-based ELISA protocols. P.L.C., P.T. and L.C. established iMGs differentiation protocol. M.H.B. supervised iMGs differentiation protocol establishment. Y.M.H.T. performed RNA quality assessment in Bioanalyzer. P.L.C. and I.J.S.F. prepared cDNA libraries prior to

RNA-sequencing. P.L.C. and C.Y.L. ran bioinformatic analyses and carried out statistical analyses. K.J.B. provided platforms for bioinformatic analysis. K.J.B. and F.M.R. supervised bioinformatic analysis. S.K.R. supervised hiPSC-derived NSCs and astrocytes differentiations and donated NSCs and astrocytes cell lines, generated in his laboratory. P.L.C. and F.M.R. prepared the manuscript. L.B.V. provided research funding. F.M.R. supervised this study and obtained research grant funding. All researchers involved in this study read, made their contribution to the final version of this manuscript and agreed to publish this work.

CONFLICT OF INTEREST

Authors declare no conflict of interest.

REFERENCES

1 Solmi, M. *et al.* Incidence, prevalence, and global burden of schizophrenia - data, with critical appraisal, from the Global Burden of Disease (GBD) 2019. *Mol Psychiatry* **28**, 5319-5327 (2023). https://doi.org:10.1038/s41380-023-02138-4

2 Hafner, H., Maurer, K., Loffler, W. & Riecher-Rossler, A. The influence of age and sex on the onset and early course of schizophrenia. *Br J Psychiatry* **162**, 80-86 (1993). https://doi.org:10.1192/bjp.162.1.80

3 Cannon, T. D. How Schizophrenia Develops: Cognitive and Brain Mechanisms Underlying Onset of Psychosis. *Trends Cogn Sci* **19**, 744-756 (2015). https://doi.org:10.1016/j.tics.2015.09.009

4 Perez, S. M. & Lodge, D. J. New approaches to the management of schizophrenia: focus on aberrant hippocampal drive of dopamine pathways. *Drug Des Devel Ther* **8**, 887-896 (2014). https://doi.org:10.2147/DDDT.S42708

5 Sakurai, T. *et al.* Converging models of schizophrenia--Network alterations of prefrontal cortex underlying cognitive impairments. *Prog Neurobiol* **134**, 178-201 (2015). https://doi.org:10.1016/j.pneurobio.2015.09.010

6 Hilker, R. *et al.* Heritability of Schizophrenia and Schizophrenia Spectrum Based on the Nationwide Danish Twin Register. *Biol Psychiatry* **83**, 492-498 (2018). https://doi.org:10.1016/j.biopsych.2017.08.017

7 Lipner, E., Murphy, S. K. & Ellman, L. M. Prenatal Maternal Stress and the Cascade of Risk to Schizophrenia Spectrum Disorders in Offspring. *Curr Psychiatry Rep* **21**, 99 (2019). https://doi.org:10.1007/s11920-019-1085-1

8 Muller, N., Weidinger, E., Leitner, B. & Schwarz, M. J. The role of inflammation in schizophrenia. *Front Neurosci* **9**, 372 (2015). https://doi.org:10.3389/fnins.2015.00372

9 Nimgaonkar, V. L., Prasad, K. M., Chowdari, K. V., Severance, E. G. & Yolken, R. H. The complement system: a gateway to gene-environment interactions in schizophrenia pathogenesis. *Mol Psychiatry* **22**, 1554-1561 (2017). https://doi.org:10.1038/mp.2017.151

10 Frydecka, D. *et al.* Profiling inflammatory signatures of schizophrenia: A cross-sectional and meta-analysis study. *Brain Behav Immun* **71**, 28-36 (2018). https://doi.org:10.1016/j.bbi.2018.05.002

11 Rodrigues-Amorim, D. *et al.* Cytokines dysregulation in schizophrenia: A systematic review of psychoneuroimmune relationship. *Schizophr Res* **197**, 19-33 (2018). https://doi.org:10.1016/j.schres.2017.11.023

12 Retallick-Townsley, K. G. *et al.* Dynamic stress- and inflammatory-based regulation of psychiatric risk loci in human neurons. *bioRxiv* (2024). https://doi.org:10.1101/2024.07.09.602755

13 Bernaus, A., Blanco, S. & Sevilla, A. Glia Crosstalk in Neuroinflammatory Diseases. *Front Cell Neurosci* **14**, 209 (2020). https://doi.org:10.3389/fncel.2020.00209

14 Linnerbauer, M., Wheeler, M. A. & Quintana, F. J. Astrocyte Crosstalk in CNS Inflammation. *Neuron* **108**, 608-622 (2020). https://doi.org:10.1016/j.neuron.2020.08.012

15 Liu, W., Tang, Y. & Feng, J. Cross talk between activation of microglia and astrocytes in pathological conditions in the central nervous system. *Life Sci* **89**, 141-146 (2011). https://doi.org:10.1016/j.lfs.2011.05.011

16 Vainchtein, I. D. *et al.* Astrocyte-derived interleukin-33 promotes microglial synapse engulfment and neural circuit development. *Science* **359**, 1269-1273 (2018). https://doi.org:10.1126/science.aal3589

17 de Oliveira Figueiredo, E. C., Cali, C., Petrelli, F. & Bezzi, P. Emerging evidence for astrocyte dysfunction in schizophrenia. *Glia* **70**, 1585-1604 (2022). https://doi.org:10.1002/glia.24221

18 Dietz, A. G., Goldman, S. A. & Nedergaard, M. Glial cells in schizophrenia: a unified hypothesis. *Lancet Psychiatry* **7**, 272-281 (2020). https://doi.org:10.1016/S2215-0366(19)30302-5

19 Gandal, M. J. *et al.* Transcriptome-wide isoform-level dysregulation in ASD, schizophrenia, and bipolar disorder. *Science* **362** (2018). https://doi.org:10.1126/science.aat8127

20 Kim, M. *et al.* In Vivo Reactive Astrocyte Imaging in Patients With Schizophrenia Using Fluorine 18-Labeled THK5351. *JAMA Netw Open* **7**, e2410684 (2024). https://doi.org:10.1001/jamanetworkopen.2024.10684

21 Windrem, M. S. *et al.* Human iPSC Glial Mouse Chimeras Reveal Glial Contributions to Schizophrenia. *Cell Stem Cell* **21**, 195-208 e196 (2017). https://doi.org:10.1016/j.stem.2017.06.012

22 Szabo, A. *et al.* A human iPSC-astroglia neurodevelopmental model reveals divergent transcriptomic patterns in schizophrenia. *Transl Psychiatry* **11**, 554 (2021). https://doi.org:10.1038/s41398-021-01681-4

23 Trindade, P. *et al.* Induced pluripotent stem cell-derived astrocytes from patients with schizophrenia exhibit an inflammatory phenotype that affects vascularization. *Mol Psychiatry* **28**, 871-882 (2023). https://doi.org:10.1038/s41380-022-01830-1

24 Koskuvi, M. *et al.* Contribution of astrocytes to familial risk and clinical manifestation of schizophrenia. *Glia* **70**, 650-660 (2022). https://doi.org:10.1002/glia.24131

25 Akkouh, I. A. *et al.* Derivation and Molecular Characterization of a Morphological Subpopulation of Human iPSC Astrocytes Reveal a Potential Role in Schizophrenia and Clozapine Response. *Schizophr Bull* **48**, 190-198 (2022). https://doi.org:10.1093/schbul/sbab092

26 Feinberg, I. Schizophrenia: caused by a fault in programmed synaptic elimination during adolescence? *J Psychiatr Res* **17**, 319-334 (1982). https://doi.org:10.1016/0022-3956(82)90038-3

27 Paolicelli, R. C. *et al.* Synaptic pruning by microglia is necessary for normal brain development. *Science* **333**, 1456-1458 (2011). https://doi.org:10.1126/science.1202529

28 Stevens, B. *et al.* The classical complement cascade mediates CNS synapse elimination. *Cell* **131**, 1164-1178 (2007). https://doi.org:10.1016/j.cell.2007.10.036

29 Yilmaz, M. *et al.* Overexpression of schizophrenia susceptibility factor human complement C4A promotes excessive synaptic loss and behavioral changes in mice. *Nat Neurosci* **24**, 214-224 (2021). https://doi.org:10.1038/s41593-020-00763-8

30 Trindade, P. *et al.* Short and long TNF-alpha exposure recapitulates canonical astrogliosis events in human-induced pluripotent stem cells-derived astrocytes. *Glia* **68**, 1396-1409 (2020). https://doi.org:10.1002/glia.23786

31 Moraga, I., Spangler, J., Mendoza, J. L. & Garcia, K. C. Multifarious determinants of cytokine receptor signaling specificity. *Adv Immunol* **121**, 1-39 (2014). https://doi.org:10.1016/B978-0-12-800100-4.00001-5

32 Mecca, C., Giambanco, I., Donato, R. & Arcuri, C. Microglia and Aging: The Role of the TREM2-DAP12 and CX3CL1-CX3CR1 Axes. *Int J Mol Sci* **19** (2018). https://doi.org:10.3390/ijms19010318

33 Lambert, S. A. *et al.* The Human Transcription Factors. *Cell* **172**, 650-665 (2018). https://doi.org:10.1016/j.cell.2018.01.029

34 Koskuvi, M. *et al.* Genetic contribution to microglial activation in schizophrenia. *Mol Psychiatry* (2024). https://doi.org:10.1038/s41380-024-02529-1

35 Uranova, N. A., Vikhreva, O. V. & Rakhmanova, V. I. Abnormal microglial reactivity in gray matter of the prefrontal cortex in schizophrenia. *Asian J Psychiatr* **63**, 102752 (2021). https://doi.org:10.1016/j.ajp.2021.102752

36 Sellgren, C. M. *et al.* Increased synapse elimination by microglia in schizophrenia patient-derived models of synaptic pruning. *Nat Neurosci* **22**, 374-385 (2019). https://doi.org:10.1038/s41593-018-0334-7

37 Sekar, A. *et al.* Schizophrenia risk from complex variation of complement component 4. *Nature* **530**, 177-183 (2016). https://doi.org:10.1038/nature16549

38 Schizophrenia Working Group of the Psychiatric Genomics, C. Biological insights from 108 schizophrenia-associated genetic loci. *Nature* **511**, 421-427 (2014). https://doi.org:10.1038/nature13595

39 Chamera, K., Szuster-Gluszczak, M. & Basta-Kaim, A. Shedding light on the role of CX3CR1 in the pathogenesis of schizophrenia. *Pharmacol Rep* **73**, 1063-1078 (2021). https://doi.org:10.1007/s43440-021-00269-5

40 Snijders, G. *et al.* A loss of mature microglial markers without immune activation in schizophrenia. *Glia* **69**, 1251-1267 (2021). https://doi.org:10.1002/glia.23962

41 Spittau, B. Aging Microglia-Phenotypes, Functions and Implications for Age-Related Neurodegenerative Diseases. *Front Aging Neurosci* **9**, 194 (2017). https://doi.org:10.3389/fnagi.2017.00194

42 Suryadevara, V. *et al.* SenNet recommendations for detecting senescent cells in different tissues. *Nat Rev Mol Cell Biol* (2024). https://doi.org:10.1038/s41580-024-00738-8

43 Zhao, Y., Shao, Q. & Peng, G. Exhaustion and senescence: two crucial dysfunctional states of T cells in the tumor microenvironment. *Cell Mol Immunol* **17**, 27-35 (2020). https://doi.org:10.1038/s41423-019-0344-8

44 Uranova, N. A., Vikhreva, O. V., Rakhmanova, V. I. & Orlovskaya, D. D. Dystrophy of Oligodendrocytes and Adjacent Microglia in Prefrontal Gray Matter in Schizophrenia. *Front Psychiatry* **11**, 204 (2020). https://doi.org:10.3389/fpsyt.2020.00204

45 Kaufmann, T. *et al.* Common brain disorders are associated with heritable patterns of apparent aging of the brain. *Nat Neurosci* **22**, 1617-1623 (2019). https://doi.org:10.1038/s41593-019-0471-7

46 Lin, C. W. *et al.* Older molecular brain age in severe mental illness. *Mol Psychiatry* **26**, 3646-3656 (2021). https://doi.org:10.1038/s41380-020-0834-1

47 Stone, W. S. *et al.* Neurodegenerative model of schizophrenia: Growing evidence to support a revisit. *Schizophr Res* **243**, 154-162 (2022). https://doi.org:10.1016/j.schres.2022.03.004

48 Candlish, M. & Hefendehl, J. K. Microglia Phenotypes Converge in Aging and Neurodegenerative Disease. *Front Neurol* **12**, 660720 (2021). https://doi.org:10.3389/fneur.2021.660720

49 Cosgrove, D. *et al.* Genes influenced by MEF2C contribute to neurodevelopmental disease via gene expression changes that affect multiple types of cortical excitatory neurons. *Hum Mol Genet* **30**, 961-970 (2021). https://doi.org:10.1093/hmg/ddaa213

50 Mitchell, A. C. *et al.* MEF2C transcription factor is associated with the genetic and epigenetic risk architecture of schizophrenia and improves cognition in mice. *Mol Psychiatry* **23**, 123-132 (2018). https://doi.org:10.1038/mp.2016.254

51 Shimamoto-Mitsuyama, C. *et al.* Lipid Pathology of the Corpus Callosum in Schizophrenia and the Potential Role of Abnormal Gene Regulatory Networks with Reduced Microglial Marker Expression. *Cereb Cortex* **31**, 448-462 (2021). https://doi.org:10.1093/cercor/bhaa236

52 Zhu, Z. H. *et al.* Association between the HHEX polymorphism and delayed memory in first-episode schizophrenic patients. *Schizophr Res Cogn* **36**, 100304 (2024). https://doi.org:10.1016/j.scog.2024.100304

53 Jaffe, A. E. *et al.* Mapping DNA methylation across development, genotype and schizophrenia in the human frontal cortex. *Nat Neurosci* **19**, 40-47 (2016). https://doi.org:10.1038/nn.4181

54 de Lima, I. B. Q. *et al.* Blockade of mGluR5 in astrocytes derived from human iPSCs modulates astrocytic function and increases phagocytosis. *Front Immunol* **14**, 1283331 (2023). https://doi.org:10.3389/fimmu.2023.1283331

55 Sellgren, C. M. *et al.* Patient-specific models of microglia-mediated engulfment of synapses and neural progenitors. *Mol Psychiatry* **22**, 170-177 (2017). https://doi.org:10.1038/mp.2016.220

56 Villasana, L. E., Klann, E. & Tejada-Simon, M. V. Rapid isolation of synaptoneurosomes and postsynaptic densities from adult mouse hippocampus. *J Neurosci Methods* **158**, 30-36 (2006). https://doi.org:10.1016/j.jneumeth.2006.05.008

57 Sheehan, D. V. *et al.* The Mini-International Neuropsychiatric Interview (M.I.N.I.): the development and validation of a structured diagnostic psychiatric interview for DSM-IV and ICD-10. *J Clin Psychiatry* **59 Suppl 20**, 22-33;quiz 34-57 (1998).

58 Ohgidani, M. *et al.* Direct induction of ramified microglia-like cells from human monocytes: dynamic microglial dysfunction in Nasu-Hakola disease. *Sci Rep* **4**, 4957 (2014). https://doi.org:10.1038/srep04957

59 Hilsenbeck, O. *et al.* fastER: a user-friendly tool for ultrafast and robust cell segmentation in large-scale microscopy. *Bioinformatics* **33**, 2020-2028 (2017). https://doi.org:10.1093/bioinformatics/btx107

60 Stirling, D. R. *et al.* CellProfiler 4: improvements in speed, utility and usability. *BMC Bioinformatics* **22**, 433 (2021). https://doi.org:10.1186/s12859-021-04344-9

61 Yang, K., Zhou, Y., Roberts, B. L., Nie, X. & Tang, W. Evaluation of the binding affinity of E3 ubiquitin ligase ligands by cellular target engagement and in-cell ELISA assay. *STAR Protoc* **2**, 100288 (2021). https://doi.org:10.1016/j.xpro.2020.100288

62 Leng, K. *et al.* CRISPRi screens in human iPSC-derived astrocytes elucidate regulators of distinct inflammatory reactive states. *Nat Neurosci* **25**, 1528-1542 (2022). https://doi.org:10.1038/s41593-022-01180-9

63 Lachmann, A. *et al.* Massive mining of publicly available RNA-seq data from human and mouse. *Nat Commun* **9**, 1366 (2018). https://doi.org:10.1038/s41467-018-03751-6

64 Espuny-Camacho, I. *et al.* Pyramidal neurons derived from human pluripotent stem cells integrate efficiently into mouse brain circuits in vivo. *Neuron* **77**, 440-456 (2013). https://doi.org:10.1016/j.neuron.2012.12.011

65 Molla Kazemiha, V. *et al.* PCR-based detection and eradication of mycoplasmal infections from various mammalian cell lines: a local experience. *Cytotechnology* **61**, 117-124 (2009). https://doi.org:10.1007/s10616-010-9252-6

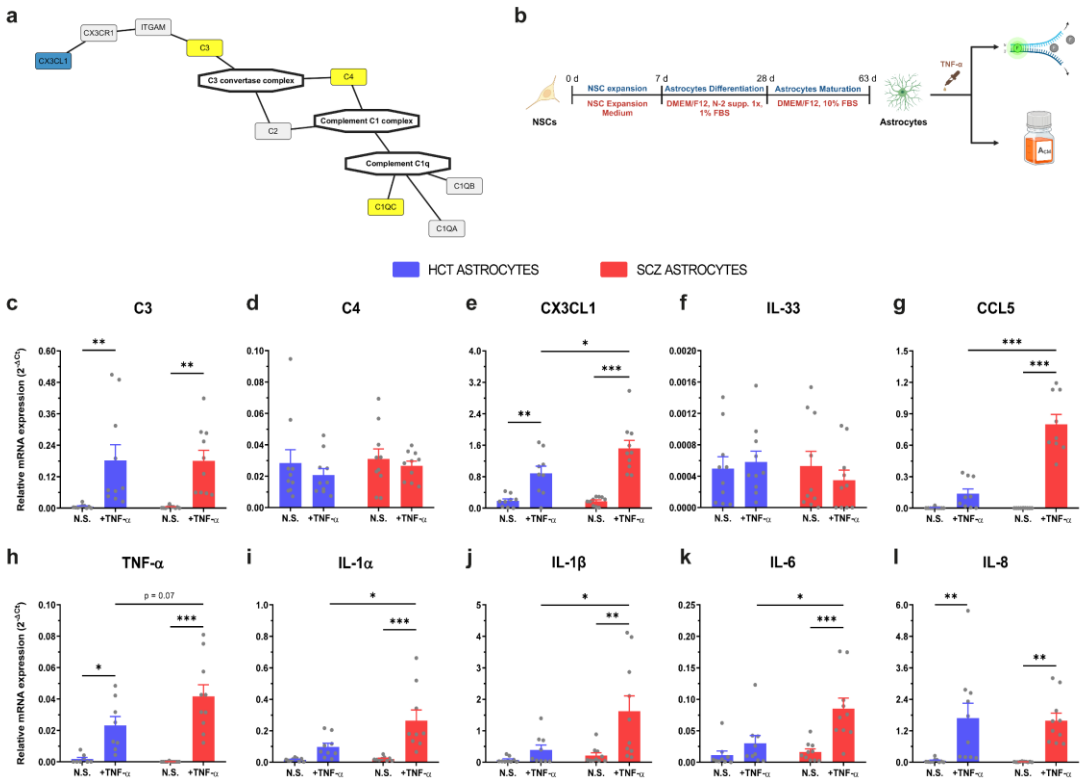

FIGURE 1: SCZ astrocytes showed stronger pro-inflammatory response upon TNF-α stimulation. a Synaptic pruning proteins network, highlighting CX3CL1 (blue) and classical complement components (yellow): C1q (subunit C), C3 and C4. Macromolecular complexes are drawn as hexagons and individual proteins as round rectangles. **b** Experimental design of hiPSC-derived astrocytes differentiation, stimulation with TNF-α (10 ng/mL) and downstream assays (RT-qPCR and conditioned media harvest for further applications). *Schematic picture was drawn on Biorender*. **c-l** mRNA expression of C3 **(c)**, C4 **(d),** CX3CL1 **(e),** IL-33 **(f),** CCL5 **(g),** TNF-α **(h),** IL-1α **(i),** IL-1β **(j)**, IL-6 **(k)** and IL-8 **(l)** in HCT and SCZ astrocytes stimulated with TNF-α. *n = 8-10 (two replicates x number of donor cell lines per group). Data were analysed by Two-way ANOVA, followed by Sidak's multiple comparison test. Bars represent Mean ± SEM. * p < 0.05, ** p < 0.01, *** p < 0.001.*

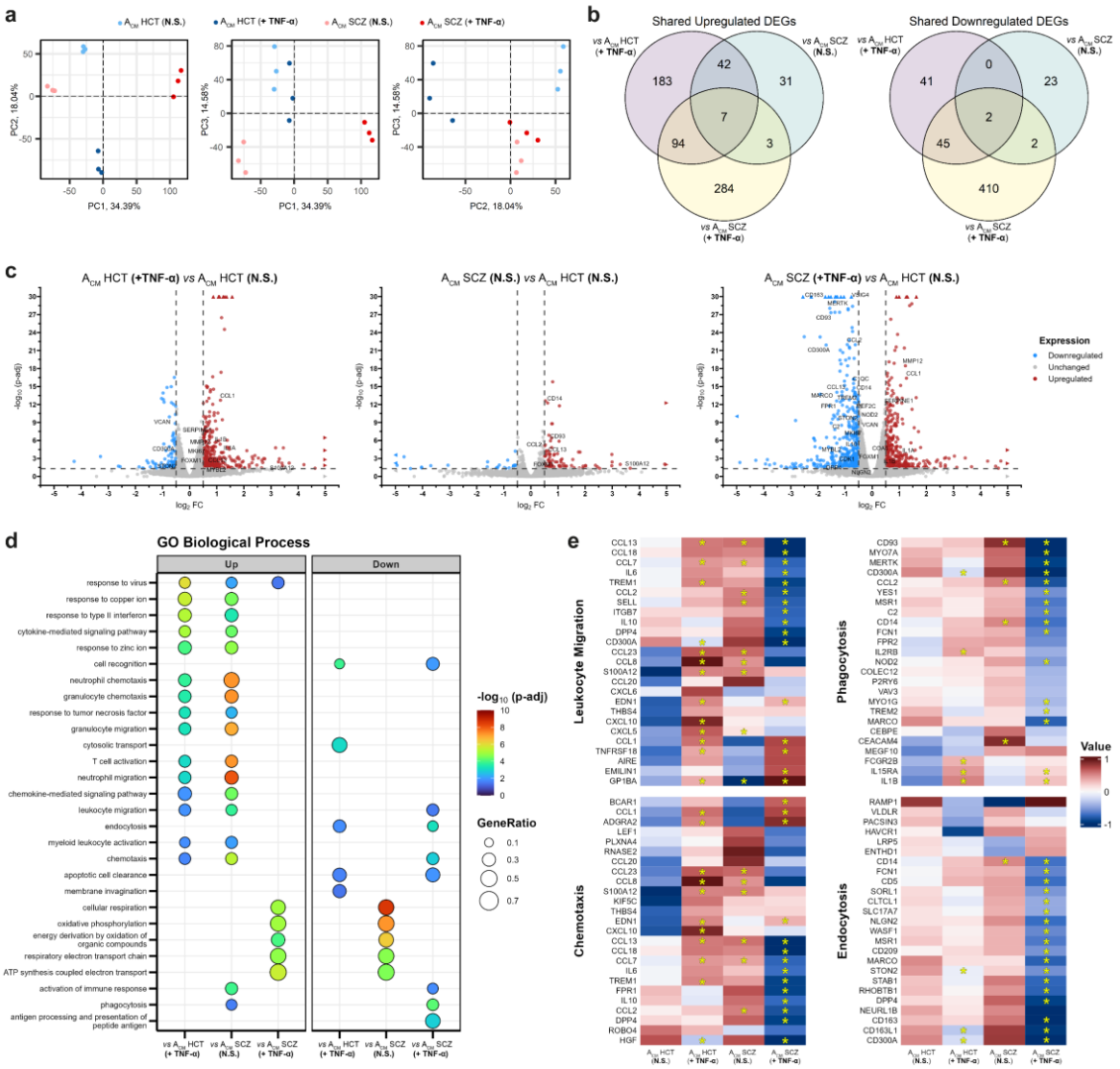

FIGURE 2: iMGs displayed divergent transcriptional profile when incubated with A_{CM} from TNF-α-stimulated SCZ astrocytes. a Principal component (PC) analysis of iMG samples incubated with all four distinct A_{CM} sources. (*left*) PC1 x PC2; (*middle*) PC1 x PC3; (*right*) PC2 x PC3. **b** Venn diagrams showing shared upregulated (*left*) and downregulated (*right*) DEGs between iMGs exposed to A_{CM} HCT (+TNF-α), A_{CM} SCZ (N.S.) or A_{CM} SCZ (+TNF-α). **c** Volcano plot depicting DEGs in iMGs cultured with: (*left*) A_{CM} HCT (+TNF-α) vs A_{CM} HCT (N.S.), (*middle*) A_{CM} SCZ (N.S.) vs A_{CM} HCT (N.S.), and (*right*) A_{CM} SCZ (+TNF-α) vs A_{CM} HCT (N.S.). Upregulated and downregulated DEGs are coloured in red and blue, respectively. Circles and triangles indicate genes within and out of the plot axes range, respectively. **d** Gene-set enrichment analysis (GSEA) plot results presenting the most relevant GO Biological Processes associated with each experimental condition. *vs means that the indicated analysis is expressed relative to iMGs + A_{CM} HCT (N.S.).* **e** Heatmaps indicating relative gene expression levels in iMGs after incubation with A_{CM} HCT (N.S.), A_{CM} HCT (+TNF-α), A_{CM} SCZ (N.S.) or A_{CM} SCZ (+TNF-α). Each plot indicates the top 25 genes associated with the following GO terms: *Leukocyte Migration, Chemotaxis, Phagocytosis* and *Endocytosis*. Genes associated with distinct GO terms may be displayed more than once. *Data are displayed as mean-centred values. Yellow asterisks indicate differentially expressed genes (adjusted p-value < 0.05; $|\log_2 FC| \geq 0.5$).*

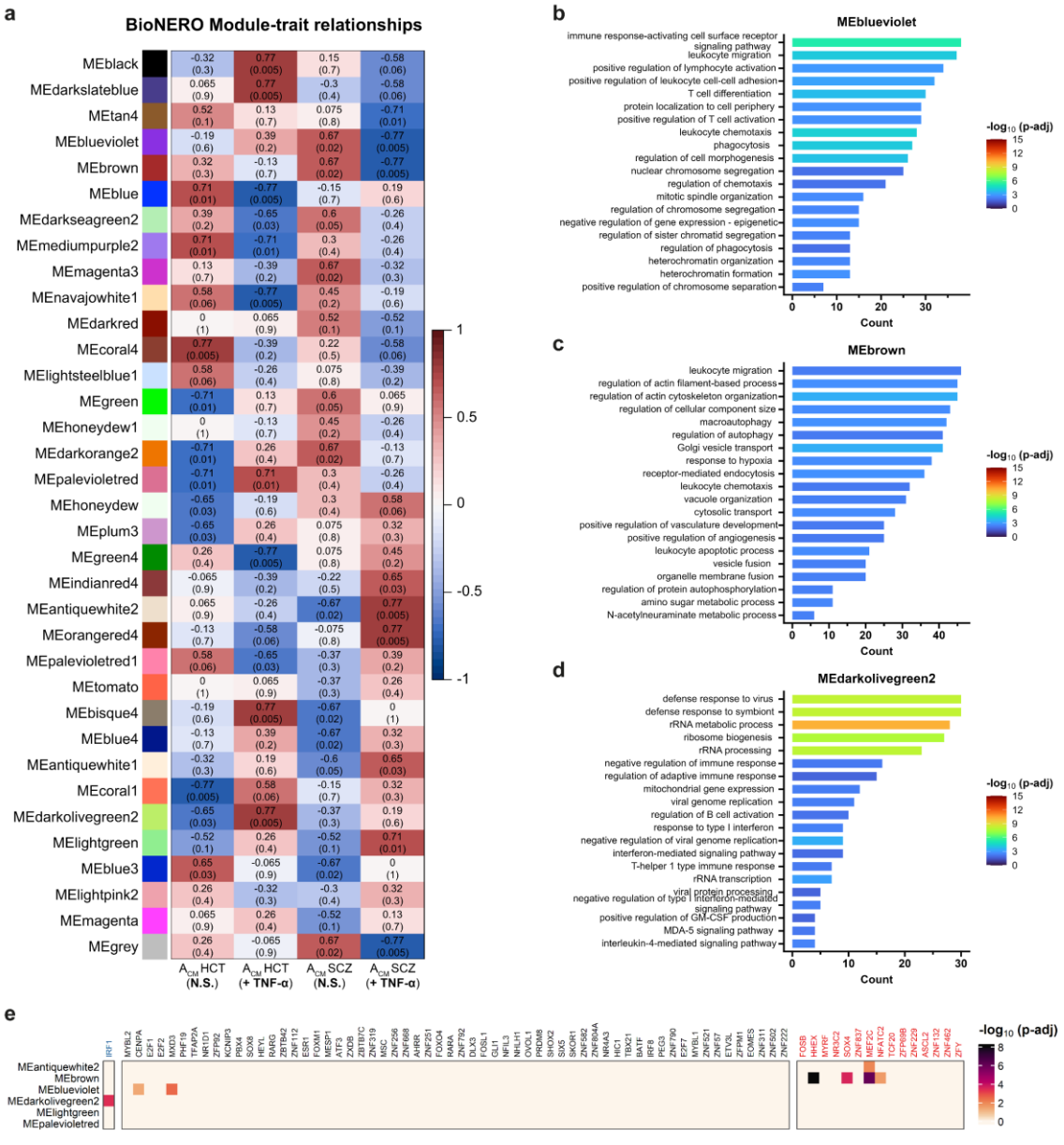

Figure 3: Identification of putative transcription factors that regulate co-expressed gene networks associated with cell migration and phagocytosis. **a** Module-trait relationships heatmap displaying the correlation between WGCNA co-expression module eigengenes and each experimental condition (i.e., iMGs + indicated A_{CM}). *Numbers in parentheses indicate adjusted p-values; above them are shown correlation values*. **b-d** Top 20 GO Biological Processes enriched in the blueviolet **(b)**, brown **(c)** and darkolivegreen2 **(d)** WGCNA modules. **e** *In silico* master regulator analysis depicting putative transcription factors, whose predicted target genes showed significant overlap with the indicated WGCNA modules gene set. *Column names in blue or red indicate master regulators related exclusively to either iMGs + A_{CM} HCT (+TNF-α) or iMGs + A_{CM} SCZ (+TNF-α), respectively, while regulons shared by at least two experimental conditions are shown in black.*

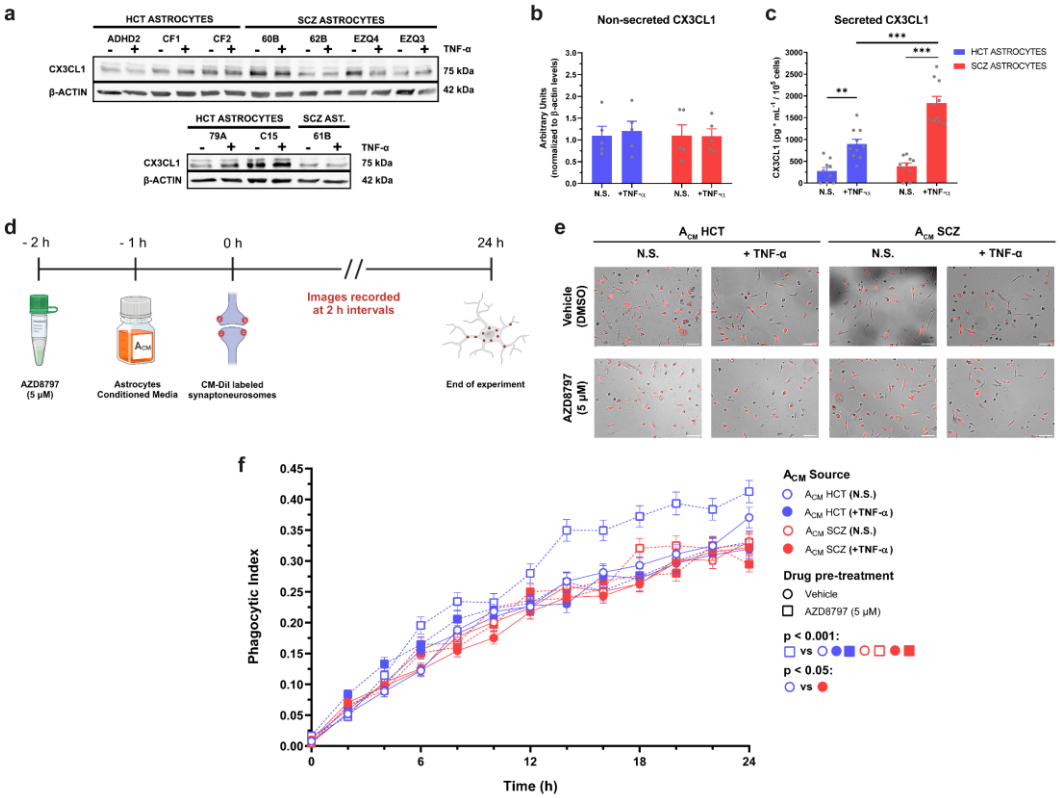

FIGURE 4: TNF-α-stimulated SCZ astrocytes secreted higher levels of CX3CL1 and impaired synaptoneurosomes engulfment by iMGs. a,b Representative Western blot of non-secreted CX3CL1 in HCT and SCZ astrocytes stimulated with 10 ng/mL TNF-α **(a)** and its respective quantification **(b)**. *Representative blot out of three independent experiments. Data are expressed relative to non-stimulated HCT astrocytes. CX3CL1 levels were normalized relative to β-actin and displayed in arbitrary units. n = 5 (number of donor cell lines per group).* **c** Secreted CX3CL1 levels in HCT and SCZ astrocytes stimulated with TNF-α. *n = 10 (two replicates x number of donor cell lines per group). Data were analysed by Two-way ANOVA, followed by Sidak's multiple comparison test. Bars represent Mean ± SEM. * p < 0.05, ** p < 0.01, *** p < 0.001.* **d** Experimental design of synaptoneurosomes phagocytosis assay by iMGs after pre-treatment with AZD8797 (5 μM) and exposure to A_{CM}. *Schematic picture was drawn on Biorender.* **e** iMGs (bright field) engulfing CM-DiI-labelled synaptoneurosomes (red) upon incubation with A_{CM} and after pre-treatment with the CX3CR1 antagonist AZD8797. Panel depicting 16 h time-point. *Scale bar = 100 μm.* **f** Quantification of synaptoneurosomes uptake by iMGs incubated with A_{CM} and pre-treated with AZD8797 depicted in **(e)** and **(Supplementary Figure 8)**. Blue symbols: A_{CM} from HCT astrocytes; red symbols: A_{CM} from SCZ astrocytes; open symbols: A_{CM} from non-stimulated astrocytes; filled symbols: A_{CM} from TNF-α-stimulated astrocytes; circles and solid lines: vehicle (DMSO)-treated iMGs; squares and dashed lines: AZD8797-treated iMGs. *n = 355-744 (number of cells in 4 different fields of two independent experiments). Data were analysed by Multilevel Mixed-effects linear regression, followed by Sidak's multiple comparison test. Symbols represent Mean ± SEM. Pairwise significant comparisons are shown at the right side of the plot.*

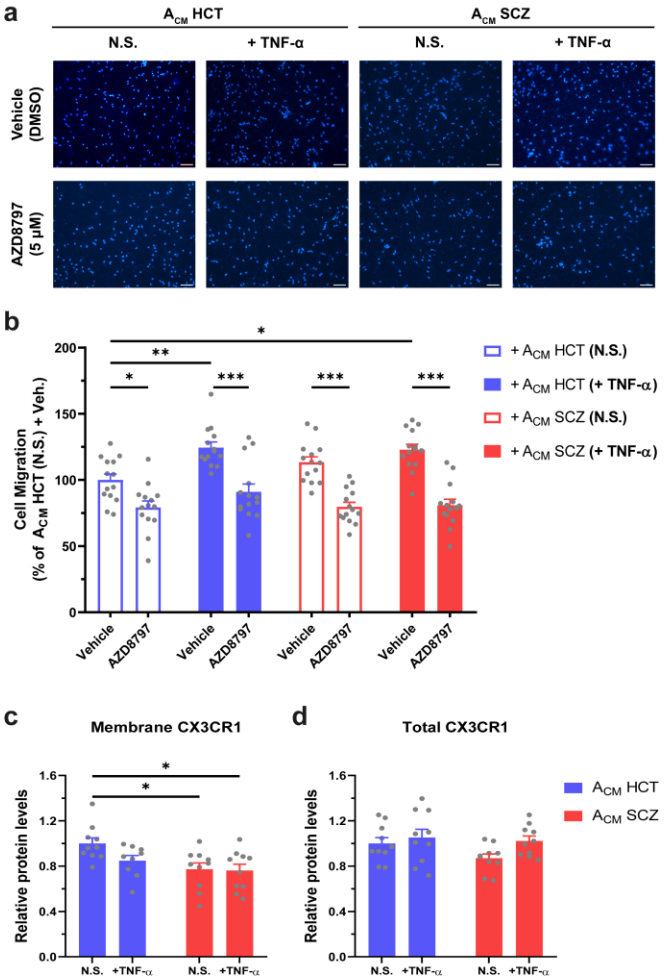

FIGURE 5: TNF-α-stimulated astrocytes promoted iMGs' migration. a Migrated iMGs after overnight incubation with A_{CM} and pre-treatment with either vehicle (DMSO) or the CX3CR1 antagonist AZD8797 (5 μM). Nuclei were stained with Hoechst (blue). *Scale bar = 100 μm.* **b** Quantification of iMGs' migration shown in **(a)**. *n = 14 (4-5 fields per transwell x number of transwells per group). Data were normalized relative to the percentage of migrated iMGs in vehicle-treated cells cultured overnight in the presence of A_{CM} HCT (N.S.). Data were analysed by Three-way ANOVA, followed by Sidak's multiple comparison test. Bars represent Mean ± SEM.* **c,d** CX3CR1 relative protein levels measured in the plasma membrane **(c)** and in the whole cell **(d)** in iMGs incubated with A_{CM} for 24 h. *n = 9-10 (number of replicates in two independent experiments). Data were analysed by Two-way ANOVA, followed by Sidak's multiple comparison test. Bars represent Mean ± SEM. * $p < 0.05$, ** $p < 0.01$, *** $p < 0.001$.*